Molecular Crystals and Liquid Crystals Science and Technology. Section A. Molecular Crystals and Liquid Crystals

Publication details, including instructions for authors and subscription information:
http://www.tandfonline.com/loi/gmcl19

Transient Stripe Patterns of Nematics in a Continuously Rotating Magnetic Field

Maren Grigutsch [a] & Ralf Stannarius [a]

[a] Universität Leipzig, Fakultät für Physik und Geowissenschaften, Linnéstr. 5, Leipzig, 04103, Germany

Version of record first published: 04 Oct 2006

To cite this article: Maren Grigutsch & Ralf Stannarius (1997): Transient Stripe Patterns of Nematics in a Continuously Rotating Magnetic Field, Molecular Crystals and Liquid Crystals Science and Technology. Section A. Molecular Crystals and Liquid Crystals, 304:1, 455-461

To link to this article: http://dx.doi.org/10.1080/10587259708046996

Mol. Cryst. Liq. Cryst., 1997, Vol. 304, pp. 455–461
Reprints available directly from the publisher
Photocopying permitted by license only

TRANSIENT STRIPE PATTERNS OF NEMATICS IN A CONTINUOUSLY ROTATING MAGNETIC FIELD

MAREN GRIGUTSCH and RALF STANNARIUS
Universität Leipzig, Fakultät für Physik und Geowissenschaften
Linnéstr. 5, Leipzig, 04103, Germany

Abstract

We investigate periodically amplified transient stripe textures which are spontaneously formed in the asynchronous reorientation regime of a thin homeotropic NLC layer exposed to an in-plane continuously rotating magnetic field. Wavelengths, orientations and ranges of existence of the stripe texture are determined by means of polarizing microscopy. A theoretical model is given which incorporates *backflow* coupling and stochastic noise. The model eluciates the hydrodynamic pattern formation mechanism and describes the time-periodic characteristics of the structures in good agreement with the experiment.

PACS numbers: 61.30.Gd, 61.30.Eb, 47.20.-k, 47.54.+r

INTRODUCTION

Due to their complex but theoretically well described non-linear dynamics, nematic liquid crystals (NLC) provide interesting model systems for pattern formation outside from equilibrium. They allow well-controlled quantitative experiments. In this contribution we study a thin layer of the nematic *5CB (4-cyano-4'-pentylbiphenyl, Merck)* confined to a glass sandwich cell. Special surface treatment (lecithin coating and rubbing) of the glass substrates provides homeotropic, i.e. perpendicular anchoring for the nematic director, see Fig. 1. The initially uniform homeotropic layer is driven out of equilibrium by a horizontal continuously rotating magnetic field.

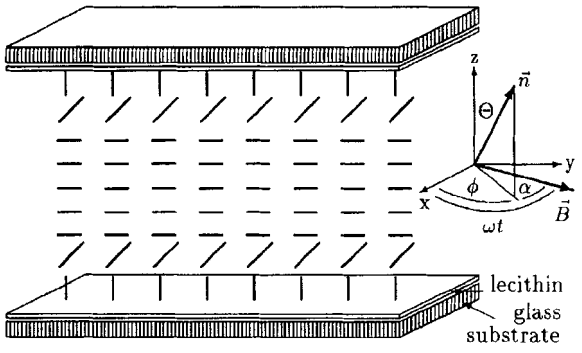

Figure 1: *Schematic drawing of the cell geometry together with the definition of the coordinate system and angles. (In the laboratory frame, the sample cell is rotated by a stepper motor in the static magnetic field.)*
cell gap: d=56μm
cell area: $1cm \times 1cm$

After the bend Fréedericksz transition, the in-plane component of the director is forced by the magnetic field to rotate about the cell normal (z-axis). The actual director response is the result of a competition between magnetic, viscous and elastic

torques. Field strength B and angular frequency ω of the magnetic field serve as control parameters. The homogeneous (with respect to the x-y plane) reorientation regime is well understood. In that case the director azimuth α with respect to the external field is given [1] by

$$\dot{\alpha} = \omega - \omega_c \sin(2\alpha) \quad \text{with} \quad \omega_c = \frac{\Delta\chi B^2}{2\mu_0 \gamma_1^*}. \tag{1}$$

γ_1^* denotes the effective rotational viscosity for the director motion and $\Delta\chi > 0$ the anisotropy of the diamagnetic suszeptibility. The critical frequency ω_c defines the transition from the synchronous state ($\omega < \omega_c$) with constant phase lag $\alpha < \pi/4$ to the asynchronous regime ($\omega > \omega_c$). In the asynchronous state, α increases monotonously with time because of strong viscous damping. In periodic phase slips the director motion slows down and reverses sense of rotation. A variety of inhomogeneous textures is generated in both reorientation regimes. Their first systematic classification was introduced by Migler and Meyer [2]. Fig. 2 presents the fundamental pattern-forming states of our system with the temperature of the sample cell stabilized to $T = 24.7°C \pm 0.1K$.

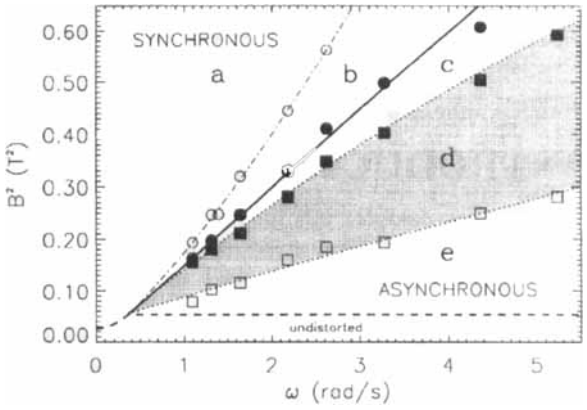

Figure 2: *Pattern-forming states of a 56μm thick homeotropic layer of 5CB at 24.7°C.*
a: static solitons,
b: dynamic solitons,
c: complex region,
d: coexistence of long-term stable VRL and time-periodic transient stripes,
e: stable VRL (see text).

The straight solid line in the B^2 vs. ω plot separates the synchronous (a,b) from the asynchronous (c-e) regime. Solitary waves (director inversion walls) in the synchronous state contain similarities to excitable phenomena in other, e.g. chemical or biological nonequilibrium systems. Recently most of their properties could be succesfully explained in the framework of a purely mechanical description of the NLC [3]. We focus on the asynchronous state where hydrodynamical effects (*backflow coupling*) play an important role in the formation of nonuniform textures. Hydrodynamic viscosity reduction has been shown [4] to be involved in the inhomogenous nucleation of director phase waves, so-called viscosity reduction lattices (VRL). An analogous mechanism was proposed to cause the spontaneous amplification of nonuniform director fluctuations leading to transient stripe patterns. Stable VRL are observed in the parameter ranges (d,e) of the state diagram (Fig. 2). In addition, quite regular stripe textures appear time-periodically within the hatched region (d). The stripes form spontaneously throughout the sample cell during the phase slip portion of each director cycle and disappear before the beginning of the next cycle. In the long-term limit, their generation is suppressed by the growth of VRL. When the experimental parameters approach the complex region (c) below the transition line to the synchronous

state, the intensity of the stripes increases considerably. In the complex state, stripe patterns of large amplitudes initiate the formation of long-term persistent nonregular director structures whereas VRL become unstable. However, the spontaneous stripes disappear abruptly when the synchronous regime is reached.

Our aim here is to characterize the stripe patterns quantitatively and to develop an analytical description of their formation. We analyze the stability of the uniform director reorientation and study the amplification mechanism of nonuniform director fluctuation modes. The model bases on the linearized hydrodynamic *Leslie-Ericksen* equations [5]. It describes the dynamics of small amplitude stripe patterns (region (d)). The correct description of the repeated and uncorrelated spontaneous formation of stripes in subsequent director cycles is finally achieved with a stochastic model that takes into account hydrodynamic noise. Theoretical predictions are compared to the experimental results.

EXPERIMENTAL RESULTS

Stripe patterns have been visualized by placing the sample cell between crossed polarizers and illuminating it from below with white light. A CCD camera mounted on a microscope was used to record the textures in the transmitted light. Typical patterns are shown in Fig. 3.

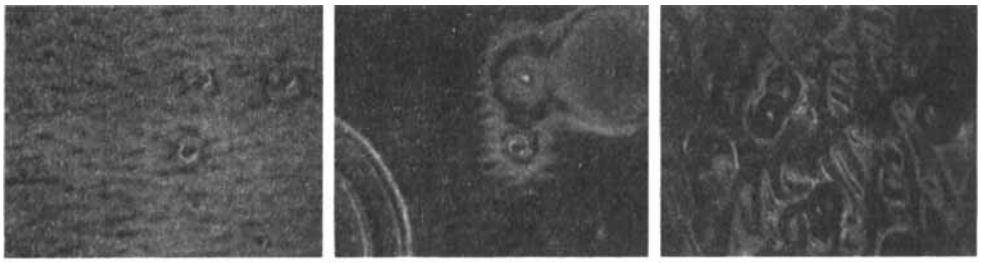

Fig. 3: *Transmission images (≈ 2.2mm× 1.6mm).* **(a):** *stripe texture in the early stage of dynamic pattern formation, B=0.543T, ω=3.18rad/s;* **(b):** *phase waves (VRL) nucleated at dust particles in competition with time-periodic stripe pattern, same parameters as previous, and* **(c):** *complex structure, B=0.64T, ω=3.27rad/s.*

The image of a well developed stripe texture in Fig. 3a was taken within the first cycles after the start of the rotation experiment. The structure momentarily covers the whole sample plane. Later on VRL begin to grow, but transient stripe textures appear simultaneously in homogeneous parts of the layer (Fig. 3b). We investigate stripe patterns far from the influence of VRL. Pattern wavelengths and orientations are extracted numerically from 2D Fourier transforms of digitized micrographs. Experimental data for the orientation of pattern wave vectors (normal to the stripes) versus time are depicted in Figure 4. Symbols (+) mark the largest peak in the Fourier power spectrum. The director angle $\phi(t)$ of the uniform reorientation mode (according to Eq. (1)) with its characteristic 'phase slips' is added for comparison. Stripes appear in the phase slips with definite periodicity. Once they have formed, their orientation with respect to the sample cell remains nearly fixed, but it is different in

the next cycle. Subsequent patterns evolve uncorrelated to each other. Corresponding wave numbers and mode amplitudes are given in Figure 5.

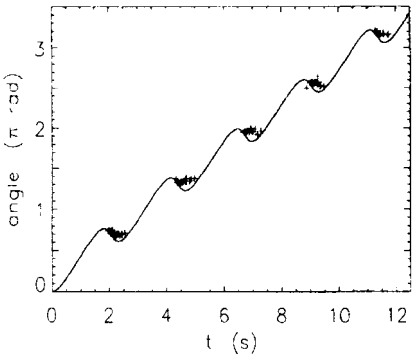

Fig. 4: *Orientation of the dominating wave vector of stripe textures (+) vs. time. The uniform director angle $\phi(t)$ (Eq. (1)) is drawn for comparison (line). ($B = 0.5T$, $\omega = 2.18 rad/s$, $T = 24.7°C$.)*

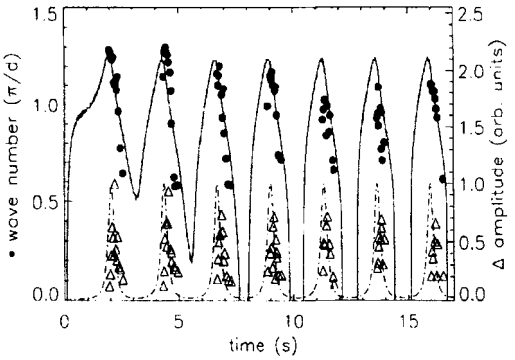

Fig. 5: *Wave number and intensity of stripes vs. time. Symbols correspond to experimental data, same parameters as Fig. 4. Lines give theoretical predictions of Eq. 10 (see next section).*

THEORY

Linear deterministic analysis

In order to describe the spontaneous anomalous amplification of nonuniform director modes we start with the hydrodynamic *Leslie-Ericksen* equations [5] and perform a linear stability analysis of the homogeneous (with respect to the xy-plane) solution for the director motion. Our analysis is greatly simplified by assuming a quasi-planar director field $\vec{n} = [\cos\phi, \sin\phi, 0]$ described adequately by its azimuthal angle $\phi(t, \vec{r}) = \overline{\phi}(t) + \varphi(t, \vec{r})$ with $\varphi(t, \vec{r})$ being a small nonuniform perturbation to the homogeneous ground state $\overline{\phi}(t)$. This assumption is justified for field strengths well above the Fréedericksz threshold ($B \gg B_F(\omega)$) where the stripe textures are actually observed in the experiments. In that limit, the director field in the sample cell is almost completely aligned in the cell plane despite of small boundary layers acting as 'slip surfaces' for the director motion. In a next approximation, we apply a quasi-two-dimensional description introducing a cell-fixed coordinate system $(x', y', z' = z)$ with the x'-axis normal to the stripes, i.e. parallel to the in-plane wave vector $\vec{q} = [q_x, q_y]$ of the pattern. After linearizing the Leslie-Ericksen equations in the distortion amplitudes we arrive at the torque balance (2) for the director distortions and the Navier-Stokes equation (3) for the related mass flow velocity $\vec{v} = u\,\vec{e_{y'}}$

$$\gamma_1 \dot{\varphi} = h(\overline{\alpha})\varphi + K(\overline{\phi}')\varphi_{x'x'} + K_2\varphi_{z'z'} - a_2(\overline{\phi}')u_{x'} \quad (2)$$

$$0 = \eta_1(\overline{\phi}')u_{x'x'} + \eta_2(\overline{\phi}')u_{z'z'} - g_2(\overline{\phi}')\varphi_{x'} + a_2(\overline{\phi}')\dot{\varphi}_{x'}\,. \quad (3)$$

The angles $\overline{\phi}'(t) = \overline{\phi}(t) - \arctan(q_y/q_x)$ and $\overline{\alpha} = \omega t - \overline{\phi}(t)$ are given by the solution of Eq. (1). As usual, we have neglected inertia terms and supposed incompressibility

of the nematic, but we retain the coupling between gradients in the director and flow fields which is essential for pattern formation in the asynchronous state. The driving magnetic field term $h(\overline{\alpha}) = -\frac{\Delta\chi}{\mu_0}B^2\cos(2\overline{\alpha})$ amplifies fluctuations in that portion of the director cycle where $(\pi/4) < \overline{\alpha} < (3\pi/4)$. In the synchronous state where always $\overline{\alpha} < \pi/4$, stripe patterns are suppressed in consistence with experimental observations. As the result of the asynchronous director rotation, the effective visco-elastic coefficients in Eqs. (2,3) become time-dependent via $\overline{\phi}'(t)$, the angle between mean orientation and gradient of the director field in the layer plane. For the definition of the coefficients we use the conventional notations [5] of Frank's elastic moduli, rotational and shear viscosities:

$$K(\overline{\phi}') = K_1\sin^2(\overline{\phi}') + K_3\cos^2(\overline{\phi}'), \qquad \eta_1(\overline{\phi}') = \eta_c\cos^2(\overline{\phi}')+\eta_b\sin^2(\overline{\phi}')+\tfrac{1}{2}\alpha_1\sin^2(2\overline{\phi}'),$$
$$a_2(\overline{\phi}') = \alpha_2\cos^2(\overline{\phi}') - \alpha_3\sin^2(\overline{\phi}'), \qquad \eta_2(\overline{\phi}') = \eta_a\cos^2(\overline{\phi}') + \eta_b\sin^2(\overline{\phi}'),$$
$$g_2(\overline{\phi}') = \gamma_2\sin(2\overline{\phi}')\,\omega_c\,\sin(2\overline{\alpha}).$$

We eliminate the flow velocity from Eq. (2) using the mode ansatz

$$\varphi_{[\vec{q},k]}(t,x',z') = A_{[\vec{q},k]}(0)\exp(\sigma_{[\vec{q},k]}(t))\sin(qx')\cos(kz') \tag{4}$$
$$u_{[q,k]}(t,x',z') = B_{[\vec{q},k]}(0)\exp(\sigma_{[\vec{q},k]}(t))\cos(qx')\cos(kz') \tag{5}$$

with real wave number q for the director and flow fields . The essential boundary condition selecting the z'-dependence is the no-slip condition for the flow field $u|_{(z'=\pm d/2)} \equiv 0$. We assume $k \approx \pi/d$ in the following (see [6] for a detailed discussion of the influence of anchoring conditions) and obtain the exponential growth rates

$$\dot{\sigma}_{\vec{q}} = \frac{1}{\overline{\gamma}_{\vec{q}}}\left\{h - Kq^2 - K_2k^2 - a_2g_2/\left(\eta_1 + \eta_2(k^2/q^2)\right)\right\}. \tag{6}$$

The reason for the anomalous amplification of nonuniform director modes is found in the wave vector dependent reduced effective viscosity

$$\overline{\gamma}_{\vec{q}}(t) = \gamma_1 - a_2^2/\left(\eta_1 + \eta_2(k^2/q^2)\right). \tag{7}$$

In the limit of small distortions where all director modes may be considered decoupled from each other, Eqs. (6,7) yield the growth rates for the full mode spectrum $\vec{q}$. Note that the effective visco-elastic coefficients are not only a function of time. They do also depend on the wave vector direction $\psi = \arctan(q_y/q_x)$ of the in-plane distortion mode under consideration. The deterministic model developed so far yields the time-evolution of the mode amplitudes

$$A_{\vec{q}}(t) = A_{\vec{q}}(0)\,\exp\left[\int_0^t \dot{\sigma}_{\vec{q}}(t')\,dt'\right]. \tag{8}$$

At a given moment t, the mode with maximum amplitude $A_{\vec{q}}(t)$ is assumed to dominate the periodicity of the texture. The model yields a quite realistic description of the first director cycle, but overestimates the damping of modes. After a few cycles nonuniform textures disappear in the simulations. In the deterministic picture, hydrodynamic noise was only considered to provide non-zero initial distortion amplitudes $A_{\vec{q}}(0)$. The continuous re-excitation of small fluctuations was neglected.

Stochastic analysis

In order to account for the influence of hydrodynamic noise we supplement the equations of motion with *Gaussian* random forces of zero average and replace amplitudes $A_{\vec{q}}$ by structure factors $C_{\vec{q}}(t) =< |A_{\vec{q}}(t)|^2 >$. After a procedure analogous to [7] we obtain

$$\frac{d}{dt}C_{\vec{q}}(t) = 2\left\{ \dot{\sigma}_{\vec{q}}(t)\, C_{\vec{q}}(t) + \frac{\epsilon}{\overline{\gamma}_{\vec{q}}(t)} \right\} \tag{9}$$

and after integration

$$C_{\vec{q}}(t) = C_{\vec{q}}(0)\, \exp\left[\int_0^t 2\,\dot{\sigma}_{\vec{q}}(t')\, dt' \right] \times \left\{ 1 + \int_0^t \frac{2\,\epsilon/\gamma_{\vec{q}}(t')\; dt'}{C_{\vec{q}}(0) \exp\left[\int_0^{t'} 2\,\dot{\sigma}_{\vec{q}}(t'')\, dt''\right]} \right\} \tag{10}$$

with the initial conditions

$$C_{\vec{q}}(0) = \frac{\epsilon}{\frac{\chi_a}{\mu_0}B^2 + K_3\, q_x^2 + K_1\, q_y^2 + K_2\, \frac{\pi^2}{d^2}}. \tag{11}$$

The parameter ϵ is a measure of the noise intensity, for example we have $\epsilon_T = 2k_BT/V \approx 10^{-12} Nm^{-2}$ for thermal noise at T=300K and sample volume $V = 56\mu m \times 1cm^2$. Figure 6 shows a contour plot of calculated structure factors (a) in comparison with the corresponding experimental mode spectrum (b). Material parameters of 5CB have been taken from literature [8].

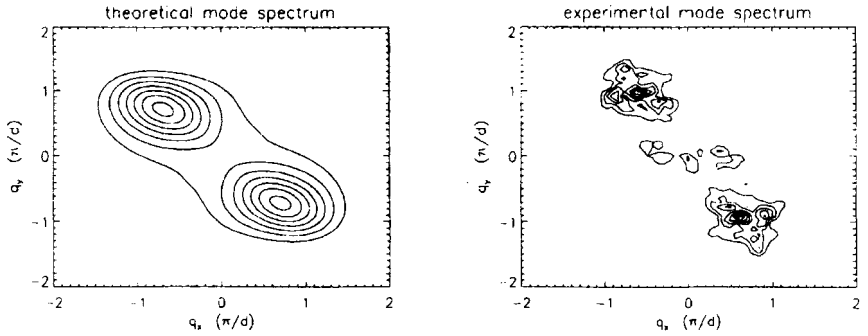

Fig. 6: *Comparison of theoretical (a) and experimental (b) mode spectra 2.2s after the start of rotation with B=0.5T and ω=2.18rad/s.*

Wave numbers and intensities of the dominating modes as function of time are presented in Fig. 5. The comparison of intensities is purely qualitative, as one has no straightforward relation between the director distortion and optical contrast. We have observed the textures between crossed polarizers at fixed angles to the magnetic field. In that case the optical contrast depends upon the mean director angle $\overline{\alpha}$ as well as upon the fluctuation amplitudes, interference and diffraction effects overlap. One notices in Fig. 5 that the experimental textures reach their maximum optical contrast only after the calculated peak of maximum fluctuation amplitude in each cycle. This may be due to the specific polarizer/analyzer geometry used in our experiments.
We arrive at the following results: The orientations, wave lengths and cyclic appearance of stripe textures are correctly reproduced within the stochastic description. Stable limit cycles are found in the simulations in accordance with the experimental

observations. In the vicinity of the synchronous state the model yields a divergence of structure factors. The patterns in the complex region (**c**) of the state diagram can be explained by superposition of large amplitude stripe patterns. To calculate their formation one has, however, to include the nonlinear coupling of large amplitude director modes which was neglected in our model. In order to explain the experimentally observed textures quantitatively, noise of much higher intensity than pure thermal noise (≈100 times larger) has to be assumed.

SUMMARY

We have presented an experimental and theoretical study of periodically generated transient stripe textures in the asynchronous reorientation of a homeotropic NLC layer exposed to a continuously rotating magnetic field. A theoretical description for the pattern formation mechanism has been given. Backflow coupling between the inhomogeneous director and mass flow fields in the nematic sample is essential for a reduced effective viscosity of director fluctuations with non-zero wave vector.
The excellent agreement between theoretical and experimental wave numbers and orientations indicates that the linearized model describes the mechanism correctly. At intermediate field strengths (region d of Fig. 2) the patterns decay before nonlinear coupling between the amplified modes can bring about additional wavelength selection mechanisms, which are characteristic for many stationary dissipative structures. A detailed theoretical and experimental study of the stripe textures and their involvement in the formation of the complex region will be given elsewhere.
The authors thank the *Deutsche Forschungsgemeinschaft* for support with grant STA 425/1.

References

1. F. Brochard; *J. Physique Lett.* **35** L19 (1974).
   F. Brochard, L. Leger, and R. B. Meyer; *J. Physique* **36** Coll C1-209 (1974).
2. K. B. Migler, and R. B. Meyer; *Phys. Rev. Lett.* **66** 1485 (1991).
3. P. Coullet, T. Frisch, J. M. Gilli, and S. Rica; *Chaos* **4** 485 (1994).
   J. M. Gilli, M. Morabito, and T. Frisch; *J. Physique II* **4** 319 (1994).
   P. Coullet, and F. Plaza; *Int. J. Bifurc. Chaos in Appl. Sci. and Eng.* **4** 1173 (1994).
   K. B. Migler, and R. B. Meyer; *Physica D* **71** 412 (1994).
   T. Frisch, S. Rica, P. Coullet, and J. M. Gilli; *Phys. Rev. Lett.* **72** 1471 (1994).
   S. Nasuno, N. Yoshimo, and S. Kai; *Phys. Rev. E* **51** (1995).
4. K. B. Migler, and R. B. Meyer; *Phys. Rev. E* **48** 1218 (1993).
5. P. G. de Gennes; *The Physics of Liquid Crystals*, Clarendon Press, Oxford 1974.
6. S. Ciaponi and S. Faetti; Liq. Cryst. **8**, 473 (1990).
7. F. Sagués, F. Arias, and M. San Miguel; Phys. Rev. A **37**, 3601 (1988), and references therein.
   F. Sagués, Phys. Rev. A **38**, 5360 (1988).
8. A. G. Chmielewski; *Mol. Cryst. Liq. Cryst.* **132** 339 (1986).
   P. A. Breddels, and J. H. C. Mulkens; *Mol. Cryst. Liq. Cryst.* **147** 107 (1987).
   K. Skarp, S. T. Lagervall, and B. Stebler; *Mol. Cryst. Liq. Cryst.* **60** 215 (1980).